# On the damped frequency response of a finite-element model of the cat eardrum

W. Robert J. Funnell
*BioMedical Engineering Unit and Department of Otolaryngology, McGill University, 3775, rue University, Montréal, Québec H3A 2B4, Canada*

Willem F. Decraemer
*Laboratorium voor Experimentele Natuurkunde, Rijksuniversitair Centrum Antwerpen, Antwerpen B-2020, Belgium*

Shyam M. Khanna
*Department of Otolaryngology, Columbia University, New York, New York 10032*

(Received 27 June 1986; accepted for publication 3 March 1987)

This article presents frequency responses calculated using a three-dimensional finite-element model of the cat eardrum that includes damping. The damping is represented by both mass-proportional and stiffness-proportional terms. With light damping, the frequency responses of points on the eardrum away from the manubrium display numerous narrow minima and maxima, the frequencies and amplitudes of which are different for different positions on the eardrum. The frequency response on the manubrium is smoother than that on the eardrum away from the manubrium. Increasing the degree of damping smooths the frequency responses both on the manubrium and on the eardrum away from the manubrium. The overall displacement magnitudes are not significantly reduced even when the damping is heavy enough to smooth out all but the largest variations. Experimentally observed frequency responses of the cat eardrum are presented for comparison with the model results.

PACS numbers: 43.63.Hx, 43.63.Bq

## INTRODUCTION

Helmholtz (1869) proposed a theory of eardrum behavior in which the peculiar curvature of the drum is important. Békésy (1941) made measurements of eardrum vibration patterns using a capacitive probe, and the results were inconsistent with Helmholtz' hypothesis. It now appeared that (at least below 2 kHz) the eardrum vibrated as a rigid body except for a small region around the periphery, and that the curvature was not particularly important. This view of eardrum behavior was predominant, in spite of some conflicting experimental observations (see review by Funnell and Laszlo, 1982), until a new set of vibration-pattern measurements were made by Khanna and Tonndorf (1972) using laser holography. These new measurements disagreed with Békésy's measurements and demanded a new theory of eardrum function. As pointed out by Khanna and Tonndorf, their data were more consistent with Helmholtz' hypothesis than with Békésy's.

Most mathematical modeling of the eardrum has involved approximating it by only two distinct rigid regions, one of which is rigidly coupled to the ossicular chain (Onchi, 1949, 1961; Zwislocki, 1957, 1962; Møller, 1961; Shaw, 1977). Such models were consistent with Békésy's view of eardrum function; they continue to be interesting because of their simplicity. Early attempts to develop the theory of eardrum vibration in more detail (Frank, 1923; Esser, 1947; Guelke and Keen, 1949; Gran, 1968) were seriously hampered by the mathematical complexity of the system. Recently a more successful analytical model has been derived using "small" parameters and asymptotic approximations (Rabbitt and Holmes, 1986a,b).

A very powerful approach to the problem has been made possible by the availability of fast digital computers, and by the development of the finite-element method, which handles a complicated system by dividing it into a large number of relatively simple parts. This is a method of analysis that has been used in engineering for more than 20 years. It is very well suited to biological problems because its strong point is its ability to handle the complexities, nonuniformities, and irregularities that abound in living systems.

The first finite-element model of the eardrum was presented by Funnell and Laszlo (1978); it was a static three-dimensional linear model for the cat. Inertial effects were added to the model and natural frequencies and mode shapes were calculated in a later paper (Funnell, 1983a). The effects of damping were not included in either of those versions of the model.

This article presents a model to which damping has been added. The definition of the model and related computational issues are discussed in Sec. I. The definition of the model includes the representation of the geometry and structure of the cat eardrum and of its attachments to the malleus, and the mechanical parameters used. The computational issues include, among other things, the implementation of a uniform pressure stimulus, as opposed to the simpler but less realistic torque stimulus that was used in a preliminary study of the effects of damping (Funnell, 1983b).

 0001-4966/87/061851-09$00.80  

Section II contains the simulation results. The steady-state behavior of the model is compared to the behavior of the earlier static model. Frequency responses with light damping are compared to the natural frequencies of an undamped model. The effects of changing the type and magnitude of the damping are investigated. Calculated frequency responses are compared to frequency responses measured experimentally in the cat ear. The effects of changing the ossicular load are calculated. Frequency responses calculated using a torque stimulus are compared to those calculated using a uniform sound pressure over the eardrum as the stimulus.

## I. METHODS

### A. Definition of the model

Except for the addition of the damping terms, the model used here is identical to the one used previously (Funnell, 1983a). The material of the eardrum is modeled as uniform and isotropic, ignoring possible mechanical implications of the highly organized layered structure of the eardrum (Funnell and Laszlo, 1982; Rabbitt and Holmes, 1986a,b). Also ignored are thickness variations, inhomogeneities such as blood vessels, and so on. The part of the model corresponding to the pars tensa (see Fig. 1) has a thickness of 40 $\mu$m, a Young's modulus of $200\times10^8$ dyn/cm$^2$, a Poisson's ratio of 0.3, and a density of 1 g/cm$^3$. The pars flaccida is modeled as being much less stiff than the pars tensa. The ligament separating the pars tensa from the pars flaccida is the same material as the pars tensa but is 300 $\mu$m thick. The drum's three-dimensional curvature is expressed by a "normalized radius of curvature" of 1.19 (Funnell, 1983a). The manubrium is constrained, by "slaving" its nodes to those on the axis of rotation, to be perfectly rigid. The ossicular load (including the effects of the malleus, incus and stapes, the middle-ear ligaments and muscles, and the cochlea) is an angular stiffness of 28 kdyn·cm/rad and a moment of inertia of 0.2 mg·cm$^2$, both acting about the axis of rotation; the position of this axis is fixed. (The mass of the manubrium is included in the ossicular load.) The effects of the middle-ear cavities are not represented, so the model is equivalent to an experimental preparation with open bulla and a closed sound system.

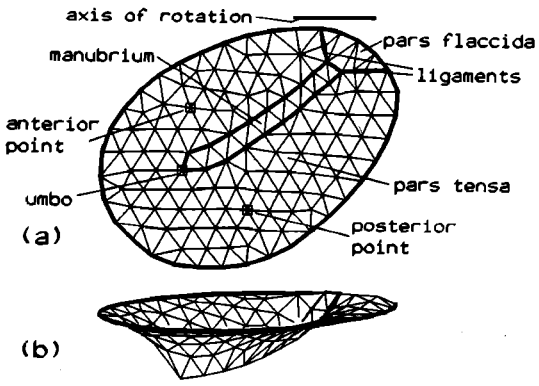


FIG. 1. Geometry of the eardrum model, with a nominal mesh resolution of 12 elements/diameter. (a) Top view. Squares indicate the positions of the anterior, posterior, and umbo points at which frequency responses have been calculated. (b) Perspective view, showing the three-dimensional curvature.

The new feature of the model is the inclusion of viscous effects, or damping. The equilibrium equation of the finite-element model is now

$$\mathbf{M}\ddot{\mathbf{u}} + \mathbf{C}\dot{\mathbf{u}} + \mathbf{K}\mathbf{u} = \mathbf{f},$$

where $\mathbf{u}$ and $\mathbf{f}$ are the vectors of nodal displacements and applied forces, respectively, and $\mathbf{M}$, $\mathbf{C}$, and $\mathbf{K}$ are the system mass, damping, and stiffness matrices.

The representation of damping being used is that of Rayleigh (or proportional) damping; that is, the effective damping matrix is given in terms of the mass matrix and stiffness matrix as

$$\mathbf{C} = \alpha\mathbf{M} + \beta\mathbf{K},$$

where $\alpha$ and $\beta$ are two damping parameters that may be specified independently (Nelson and Greif, 1975; Bathe, 1982). It can be shown that the resultant damping ratio $b$ (that is, the damping level expressed as a fraction of critical damping) is given by

$$b = (\alpha/\omega + \beta\omega)/2,$$

where $\omega$ is the angular frequency. In other words, the $\alpha$ term causes damping (expressed as a damping ratio) that decreases with frequency, while the $\beta$ term causes damping that increases with frequency. These different effects will be illustrated in Sec. II C below.

Note that, because of the way the damping is implemented in this model, the same damping coefficients apply to the ossicular load as to the eardrum itself. The $\alpha$ term causes damping with the same frequency dependence as that represented by the constant resistive damping coefficient normally associated with the ossicles and cochlea in middle-ear models.

### B. Finite-element program

As in the earlier papers, the SAP IV general-purpose finite-element package is used (Bathe *et al.*, 1974), with the addition of a "master–slave" capability for slaving certain nodes to a master node (Funnell, 1983a). The program is now being run on a VAX-11/750 computer (under the VMS operating system) rather than the PDP-11/70 used previously. This has dramatically speeded up the calculations. It also means that it has been possible to restore the use of double-precision (8-byte) floating-point arithmetic that had been removed in order to make the program fit on the PDP-11. It has been verified that the use of single-precision arithmetic did not cause large errors in previously reported results: for example, using double precision has increased the estimated lowest natural frequency by only about 2%, the second by 0.4%, and the rest by less.

### C. Stimulus

In an earlier paper (Funnell, 1983b), the damped model was driven with a step function of torque applied about the axis of rotation. This stimulus was particularly simple to implement since it could be represented as a load applied at a

single location in the model. However, the normal stimulus to the eardrum is an acoustic pressure acting over its surface, rather than a force at a single point. At low frequencies this pressure is uniform over the surface of the eardrum; at high frequencies the pressure is not uniform (Khanna and Stinson, 1985; Stinson, 1985) but the detailed pressure distribution is not known.

In this article the stimulus will be a step function of pressure applied uniformly over the surface of the drum. For the purposes of the finite-element software, this pressure must be translated into a set of forces normal to the surface:

$$\mathbf{f} = \sum \frac{p\mathbf{A}}{3},$$

where $\mathbf{f}$ is the three-dimensional force vector applied to a given node, $p$ is the pressure, and the summation is over all of the elements attached to the given node. Here $\mathbf{A}$ is a vector normal to the element with a length proportional to the element area, calculated using a vector cross product:

$$\mathbf{A} = (\mathbf{x}_2 - \mathbf{x}_1) \times (\mathbf{x}_3 - \mathbf{x}_1)/2,$$

where $\mathbf{x}_1$, $\mathbf{x}_2$, and $\mathbf{x}_3$ are the coordinate vectors of the three nodes of the triangular element. The forces are calculated by a pre-processor program and fed to the SAP IV program.

The pressure stimulus has been fixed at 100 dB SPL for all of the calculations in this article.

### D. Direct time integration

The introduction of damping into the model means that one can no longer use the procedures of matrix inversion and eigenvalue extraction that were used for the static and natural-frequency calculations. The SAP IV program offers two alternative approaches to calculating damped responses: either superposition of the previously calculated undamped natural modes, or direct time-domain integration. The superposition method is computationally cheaper if a reasonably small number of modes is adequate to represent the system response, but the fact that the natural frequencies of the eardrum model are very closely spaced means that a large number would have to be included. The direct-integration method is therefore better in the present application. In SAP IV, the integration is done using the Wilson $\theta$ method, which is unconditionally stable. The method effectively low-pass filters the response, with the degree of filtering depending on the size of the time step used for the time-domain computations. The effects of changing the size of the time step will be discussed in Sec. I F below. Details of the implementation are given in the Appendix.

### E. Frequency characteristics

The frequency response of a selected node is calculated by differentiating the step response to form an impulse response and then doing a Fourier transform. The differentiation is done using the forward difference equation

$$x_i' = (-x_{i+2} + 4x_{i+1} - 3x_i)/2\Delta t.$$

The Fourier transform is done using a mixed-radix FFT (Singleton, 1979) which does not require that the number of samples be a power of 2, only that it be a multiple of 2. The only modification to the FFT program as distributed by the IEEE has been to increase the size of the array that can be handled.

For the results presented here, the time-domain simulation was usually continued until the oscillation of the step response had settled to within less than 0.1% of the final value before calculating the frequency response. However, the frequency characteristics are in fact changed only very little even if the step response is terminated when the amplitude of the oscillation is still several percent of the final value.

Note that the model results are expressed in terms of the components of the displacements perpendicular to the plane of the tympanic ring, comparable to the displacements measured experimentally by Khanna and Tonndorf (1972).

### F. Time step and mesh resolution

A critical factor in the finite-element simulations is the choice of values for the size of the time step used in the time-domain integration, and for the number of elements in the mesh. Decreasing the size of the time step or increasing the number of elements improves the accuracy of the model at the expense of rapidly increasing the computation time. It is therefore important to determine the largest time step and the coarsest mesh resolution that will give an adequate accuracy.

As mentioned above, the Wilson $\theta$ method used here for the time-domain integration effectively performs a sort of low-pass filtering of the response. It seriously reduces the contributions from modes of vibration whose periods $T(=1/f)$ are not large compared to the time step $\Delta t$ used; for example, with $\theta = 1.4$ as in SAP IV, a mode for which $\Delta t/T = 0.05$ decays by about 1% per cycle during the course of the temporal integration (Bathe, 1982). (For $\Delta t = 10\,\mu$s, for example, this figure for $\Delta t/T$ corresponds to a modal frequency of 5 kHz.) Figure 2 shows a series of frequency responses computed for a point on the eardrum away from the manubrium for various values of the time step $\Delta t$. The curves for 5 and 10 $\mu$s are practically identical. The curve at 20 $\mu$s has started to fall off faster than it should above about 12 kHz; the one at 50 $\mu$s falls off above 5 kHz and has also smeared out the details; and the one at 100 $\mu$s has smeared out even the main features. (It should be noted that it took about 45 h of computer time, spread out over 6 nights, to calculate the curve at 5 $\mu$s.) In light of these observations, the results below were all calculated with a time step of 10 $\mu$s.

As discussed in an earlier article (Funnell, 1983a), the number of triangular elements in the finite-element mesh for the eardrum is controlled by a mesh-resolution parameter, expressed as a nominal number of elements across the diameter of the model. In that article it was concluded that a resolution of 12 elements/diameter (illustrated in Fig. 1) was a reasonable choice. Figure 3 shows frequency responses for a point on the manubrium calculated with meshes of 12 and 15 elements/diameter. The two curves are extremely similar, indicating that a resolution of 12 elements/diameter is again sufficient. All results discussed below were computed with that resolution. (Frequency responses for points off the manubrium are also similar for the two different meshes,

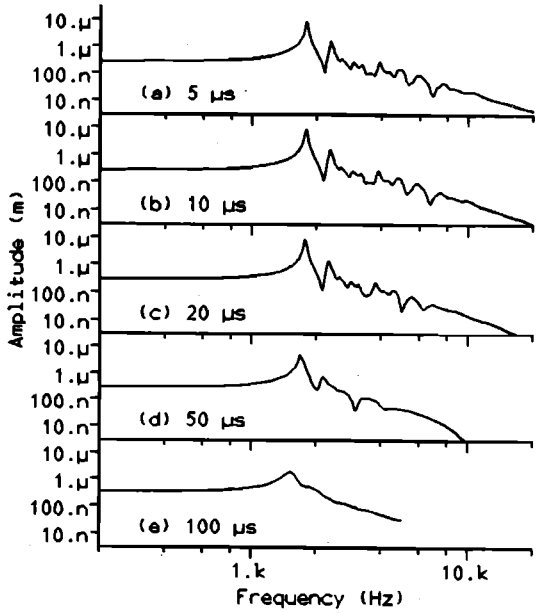


FIG. 2. Displacement frequency responses calculated with five values of the time step $\Delta t$. The frequency responses for 5, 10, and 20 $\mu$s are nearly identical, indicating that 10 $\mu$s is an acceptable step size.

but cannot be compared exactly since the positions of automatically generated nodes in the two meshes do not match exactly.)

## II. RESULTS

### A. Static displacements

The static or very-low-frequency displacement pattern of the drum is calculated using time-domain integration by computing the damped step responses at all nodes and following them out to a time large enough that the system has reached steady state. The resulting displacement contour map is shown in Fig. 4. (The same result is obtained regardless of the values of the damping parameters $\alpha$ and $\beta$.) The contours are indistinguishable visually from those calculated with the static model (Funnell, 1983a). The maximum displacement (in the posterior region of the pars tensa) is

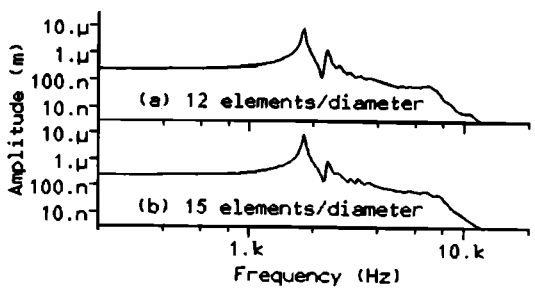


FIG. 3. Displacement frequency responses on the manubrium calculated using different mesh resolutions. (a) 12 elements/diameter. (b) 15 elements/diameter. The two are very similar, suggesting that a mesh resolution of 12 elements/diameter is adequate.

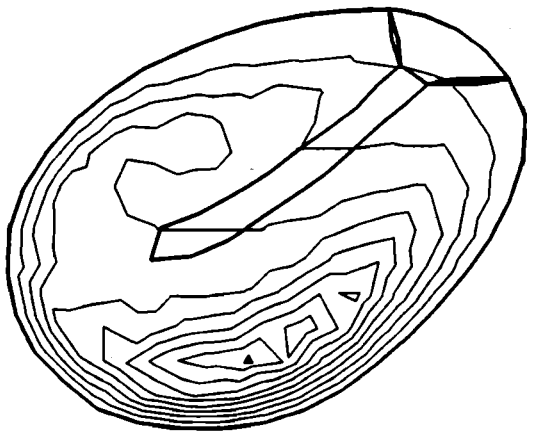

FIG. 4. Contour map of calculated static displacement amplitudes. The contours represent amplitudes evenly spaced between 0 and the maximum displacement. The position of the maximum is indicated by a filled triangle.

661.7 nm at 100 dB SPL, which is within 0.1% of the figure calculated with the static model; by comparison, Tonndorf and Khanna (1971) reported a maximal drum displacement (at 600 Hz) of 1500 nm at 111 dB SPL, corresponding to 420 nm at 100 dB SPL. The ratio of peak displacement to manubrial-tip displacement in the static case is about 2.7 for the model; Khanna and Tonndorf (1972) reported a ratio equal to 3 at low frequencies.

### B. Lightly damped responses

Figure 5 shows a set of frequency responses calculated for a case of light damping—for the solid curves the mass-proportional damping parameter $\alpha = 0\ s^{-1}$ and the stiff-

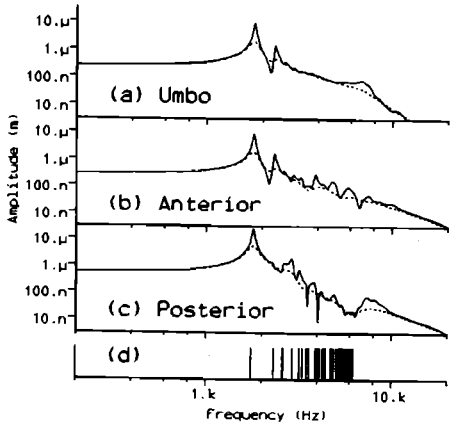


FIG. 5. Displacement frequency responses calculated with $\beta = 2\times10^{-6}$ s (solid lines) and $10\times10^{-6}$ s (dashed lines); in both cases $\alpha = 0$. Both frequency and amplitude scales are logarithmic. The model stimulus is a uniform sound pressure at 100 dB SPL. (a) Umbo. (b) Anterior point away from manubrium. (c) Posterior point away from manubrium. (d) Vertical bars representing the frequencies of the first 40 natural modes of vibration of the undamped model. The numerous narrow minima and maxima in the lightly damped frequency responses (solid lines) correspond approximately to the system's undamped natural modes. Heavier damping (dashed lines) smooths the frequency responses but does not affect their overall levels or slopes much.

ness-proportional damping parameter $\beta = 2\times10^{-6}$ s. The three sets of curves correspond to three different positions on the model. Part (a) corresponds to displacements at the umbo, on the manubrium. Parts (b) and (c) correspond to the displacements of two points on the pars tensa away from the manubrium (see Fig. 1).

The most striking feature of these frequency responses is the presence of numerous narrow minima and maxima in the curves corresponding to points away from the manubrium. These peaks and troughs correspond to the system's natural vibration modes. Their positions are different for the two points, reflecting the fact that different points on the eardrum participate differently in the various natural modes of vibration. For example, in an undamped case, modes 1, 2, 5, and 6 involve mainly the posterior region of the eardrum, while modes 3 and 4 involve both the anterior and posterior regions (Funnell, 1983a). Furthermore, one point on the drum may be at or near the place of maximal displacement for a given mode, resulting in a peak in the frequency response for the point at the frequency corresponding to that mode, while another point in the same region may happen to lie near a line of zero displacement for that mode, resulting in a trough at the same frequency.

Part (d) of Fig. 5 shows the natural frequencies corresponding to the first 40 *undamped* natural modes of vibration of the model. [This is an extension of the results of Funnell (1983a), where only the first six natural frequencies were calculated.] As a general principle, lightly damped natural modes will occur at frequencies similar to those of the corresponding undamped modes, but shifted slightly due to the damping.

For the point on the manubrium [part (a) of Fig. 5] it is striking how much the narrow minima and maxima have been smoothed out. It is evident that the nature of the manubrium's coupling to the eardrum serves to integrate the contributions of different parts of the structure. The resultant smoothing effect is powerful precisely because the different local modes are numerous and closely spaced in frequency, so they tend to cancel each other out.

### C. Effects of modifying damping

There are few experimental data available on which to base an estimate of the actual degree of damping in the eardrum, or indeed in any collagenous material, especially at high frequencies. Witnauer and Palm (1961) estimated a damping parameter of $10^3\ s^{-1}$ for leather (which is collagenous) at 15 to 20 Hz. That the degree of damping decreases with increasing frequency is suggested by measurements at up to 100 Hz in samples of eardrum tissue (Decraemer *et al.*, 1980) which showed a viscoelastic restoring force which increased only slowly with frequency. This is consistent with some very indirect evidence that the viscosity of the ground substance in collagenous tissue may decrease with increasing shear rate or frequency (Wilkes *et al.*, 1973).

In view of the lack of an experimental basis for specifying the damping parameters, we have tried a range of values for $\alpha$ and $\beta$. To begin with, the dashed lines in Fig. 5 show the frequency responses obtained by increasing the stiffness-proportional parameter $\beta$ from $2\times10^{-6}$ to $10\times10^{-6}$ s, leaving the mass-proportional parameter $\alpha$ at 0. It can be seen that increasing the damping has smoothed the frequency responses, lowering the peaks and raising the troughs. All but the largest local fluctuations have disappeared. The overall levels and slopes of the frequency responses have changed very little, and the low-frequency amplitude in particular has not changed at all. (In general, the effect of damping, unless it is extremely heavy, is seen mainly in the neighborhoods of resonances and antiresonances. This can be observed in the behavior of a simple second-order mass–spring–dashpot, or inductor–capacitor–resistor, system.)

Figure 6 shows the results of setting $\beta$ to 0 s and giving $\alpha$ values of $1.5\times10^3$, $5\times10^3$, and $10\times10^3\ s^{-1}$. The value of $1.5\times10^3\ s^{-1}$ for $\alpha$ was chosen to give roughly the same

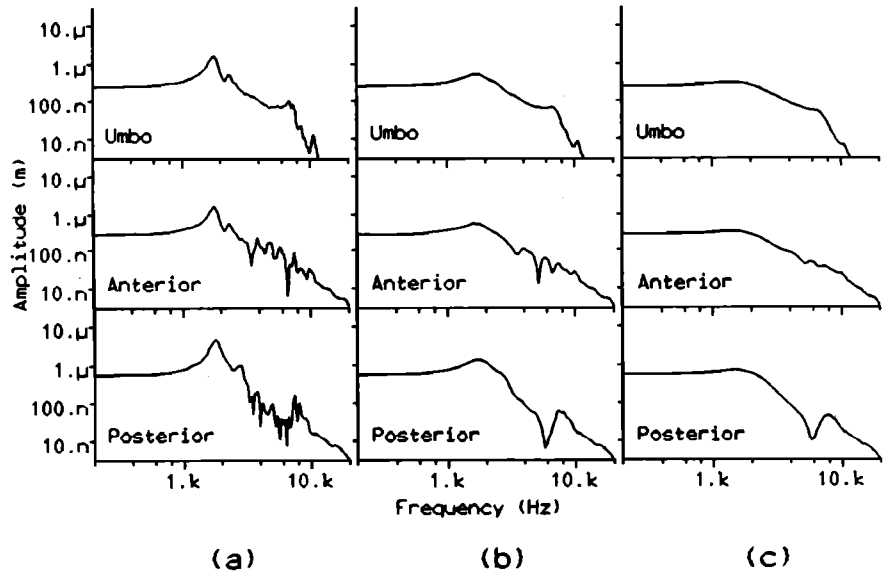


FIG. 6. Displacement frequency responses calculated with the stiffness-proportional damping parameter $\beta = 0$, and various values for the mass-proportional damping parameter $\alpha$. (a) $\alpha = 1.5\times10^3\ s^{-1}$. (b) $\alpha = 5\times10^3\ s^{-1}$. (c) $\alpha = 10\times10^3\ s^{-1}$. Increasing the damping smooths the curves more and more but leaves the overall levels and slopes unchanged.

damping ratio around 2 kHz as found for $\beta = 10 \times 10^{-6}$ s when $\alpha = 0$. It can be seen in Fig. 6(a) that the shapes of the frequency responses around 2 kHz are indeed very much like those for $\beta = 10 \times 10^{-6}$ s (Fig. 5, dashed lines). At higher frequencies, however, the damping due to $\alpha$ is lighter than at low frequencies (as discussed in Sec. I A above), and the parts of the curves above 3 kHz in Fig. 6(a) look more like the curves for the lower value of $\beta$ (Fig. 5, solid lines). Increasing $\alpha$ [Fig. 6(b) and (c)] smooths the curves more and more but leaves the overall levels and slopes unchanged, in the same way as noted for increases in $\beta$.

Figure 7 shows frequency responses measured on the manubrium and eardrum of a single cat ear using laser interferometry. (The details of the experiments will be reported in another article.) The frequency responses were measured directly using sinusoidal stimuli. The curves shown represent measurements on the manubrium at the umbo [part (a)] and at two positions on the eardrum [parts (b) and (c)]. These latter positions are approximately the same as the positions of the nodes used earlier for presenting the model results. The low-frequency amplitude on the umbo of this particular ear was about 56 nm; this is about 2.5 times smaller than the figure reported by Khanna and Tonndorf (1972), and about 4 times smaller than the figure obtained with the present model. Other animals in this experimental series yielded amplitudes about twice as large, thus agreeing more closely with the older observations.

Three separately measured frequency responses have been plotted for the point on the manubrium, and two each for the points on the eardrum. The frequency responses measured at the points on the eardrum exhibit sharp variations in amplitude, especially at high frequencies. By comparison, the frequency response measured on the manubrium is quite smooth, just as found with the model. (The large dip at 4 kHz is due to the resonance in the middle-ear cavity that is not included in the model.)

The model displays a displacement-amplitude roll-off proportional to $1/f^2$ (that is, a slope of $-12$ dB/oct) at

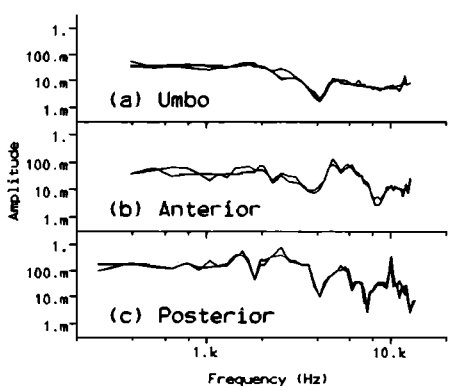


FIG. 7. Displacement frequency responses measured experimentally in cat. Both frequency and amplitude scales are logarithmic. The units are arbitrary for the amplitude scale. (a) Umbo (three separately measured curves in same ear). (b) Anterior point (two curves). (c) Posterior point (two curves). The positions of the three points correspond approximately to those used in the model.

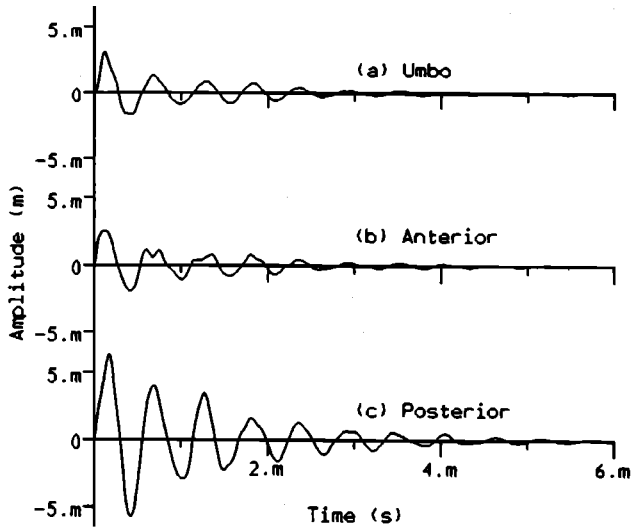


FIG. 8. Impulse responses calculated with $\alpha = 1.5 \times 10^3$ s$^{-1}$ and $\beta = 0$. Both time and amplitude scales are linear. (a) Umbo. (b) Anterior point. (c) Posterior point. The appearances of these curves are dominated by a low-frequency component at about 2 kHz.

frequencies above several kilohertz. This agrees with the measurements of Guinan and Peake (1967), for example, and indicates that mass effects are dominant at high frequencies. However, the measured cat data in Fig. 7 suggest a slower roll-off at these frequencies. Svane-Knudsen and Michelsen (1986) found the same thing in their indirect measurements in humans, as did Wilson and Johnstone (1975) in guinea pigs. The significance of this is not clear, especially in view of the difficulties in both model and experiment at high frequencies.

These experimentally observed frequency responses suggest fairly light damping, comparable to that displayed by the model when $\alpha = 1.5 \times 10^3$ s$^{-1}$ and $\beta = 0$ [Fig. 6(a)]. Figure 8 shows the impulse response of the model corresponding to these values of the damping parameters. The decay from one cycle to the next is on the order of 50%. Békésy (1960, Fig. 5-17) showed a tracing of a manubrial response to an acoustical pulse, with the amplitude decaying by about 50% to 70% from one cycle to the next. Recent impulse-response data measured in humans by Svane-Knudsen and Michelsen (1986) show a decay on the order of 30% per cycle for one subject but more like 50% for a second subject. These experimental estimates are comparable to the decay seen in the model results in Fig. 8. Note that since the gross waveform of the impulse response is dominated by frequencies around 2 kHz, these estimates of the amplitude decay give an idea only about damping in that frequency range.

### D. Effect of ossicular load

The undamped natural frequency of the ossicular load itself, calculated with the formula $f = (k/I)^{1/2}/2\pi$, where $k$ is the angular stiffness and $I$ is the moment of inertia, is 1883 Hz for the load parameters used here. This is very close to

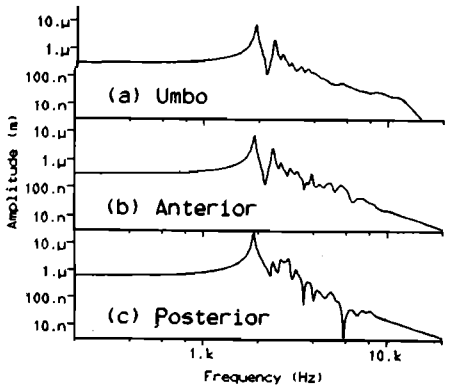


FIG. 9. Displacement frequency responses calculated after removal of ossicular load, with $\alpha = 0$ and $\beta = 2\times10^{-6}$ s. The curve corresponding to the umbo (a) has a very-low-frequency amplitude about 15% higher than the case with an ossicular load, and has lost the plateau from 5 to 7 kHz. On the other hand, the curves for points on the eardrum away from the manubrium [(b) and (c)] are quite similar to the case with an ossicular load.

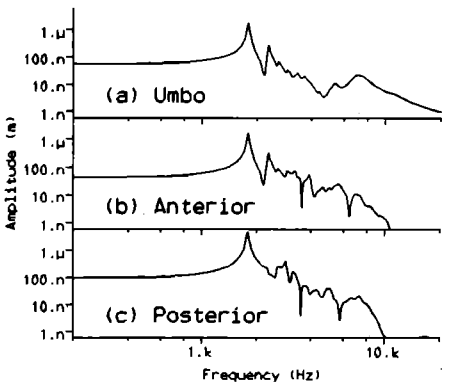


FIG. 10. Displacement frequency responses calculated with a torque of 1 dyn·cm applied to the axis of rotation, instead of a uniform pressure stimulus. The damping parameters are $\alpha = 0$ and $\beta = 2\times10^{-6}$ s, as for the solid curves in Fig. 5. Note that the vertical scale is not the same as in Fig. 5. The manubrial curve (a) drops off more slowly at high frequencies, and the off-manubrium curves (b) and (c) drop off more quickly than do the curves calculated with a pressure stimulus.

the lowest natural frequency of the overall eardrum model; the significance of this coincidence is not clear. The frequency responses shown in this article depend mainly on the eardrum itself—reducing the ossicular stiffness from 28 to 10 kdyn·cm/rad, for example, just shifts the lowest peak downward by about 100 Hz, and has even less effect at higher frequencies. This is consistent with the earlier observation that neither doubling nor halving the parameters of the ossicular load has a very large effect on the undamped natural frequencies (Funnell, 1983a).

Figure 9 shows frequency responses for the extreme case of removing the ossicular load altogether. It can be seen that there is no longer a plateau from 5 to 7 kHz in the manubrial frequency response—instead, the response continues to drop by about 12 dB/oct until past 10 kHz [part (a)]. There is also an increase of about 15% in the very-low-frequency manubrial amplitude. For the points away from the manubrium, on the other hand, the very-low-frequency amplitudes are unchanged; there are changes in the details of the curves but the overall forms are similar to those with the ossicular load, except perhaps for the posterior point [part (c)] above 5 kHz. In all three cases the peak below 2 kHz has shifted about 100 Hz to the right.

### E. Torque versus pressure

In a preliminary analysis of the effects of damping (Funnell, 1983b), the stimulus driving the eardrum model was a step of torque applied about the axis of rotation, rather than a step of pressure applied uniformly to the drum. For a comparison of the effects of these two different types of stimulus, Fig. 10 shows the frequency responses calculated with an applied torque, for the same points and model parameters as in Fig. 5. For the torque stimulus the manubrial frequency response drops off more slowly at high frequencies, and the off-manubrium responses drop off more quickly, than for the pressure stimulus. The size of this difference might be interpreted as a measure of reduced drum-manubrium coupling at high frequencies.

The experimental use of a mechanical stimulus applied directly to the manubrium might be a way to avoid the uncertainties associated with the difficult-to-quantify nonuniformity of the acoustical stimulus. The torque stimulus simulated here is equivalent to a point force applied directly to the manubrium, at least under the assumption of a fixed axis of ossicular rotation.

## III. CONCLUSIONS

The addition of the effects of damping to the finite-element model of the eardrum has permitted the simulation of dynamic forced responses for the first time. In particular, by applying step functions and then taking Fourier transforms it has been possible to compute frequency responses for the model.

The frequency responses for points on the eardrum *away from* the manubrium of the malleus tend to show sharp variations of amplitude as the frequency increases beyond about 2 kHz. These variations reflect the fact that the vibration pattern of the eardrum breaks up into complex patterns at high frequencies. For points *on* the manubrium, however, these variations are smoothed out. This is evidently the result of a sort of spatial integration over the eardrum, due to the fact that the manubrium is rigid and is coupled to the drum along its whole length. This elongated coupling, which in the cat extends over more than two thirds of the diameter of the drum, effectively averages out all but the largest local variations of response.

Increasing the degree of damping in the model reduces the amplitude variations in the frequency response, both on the manubrium and on the eardrum away from the manubrium. In fact, even a rather small amount of damping has a considerable smoothing effect. Even for a degree of damping that completely obliterates all but the very largest peaks and

troughs, the overall level of the displacement amplitude is not noticeably decreased. This suggests that damping in the eardrum results in very little loss of the energy being delivered to the middle ear.

In spite of the complex vibration patterns on the eardrum, the overall transmission of energy to the middle ear has a smooth frequency characteristic. This cannot be just because of the nature of the ossicular load, since the smoothing occurs even when there is no ossicular load at all, as shown in Fig. 9. The smoothing effects of both spatial integration and damping are very strong, due to the fact that the natural frequencies of the eardrum are very closely spaced. This in turn is partially due to the asymmetrical form of the system. If the eardrum were more symmetrical, there would be a greater tendency for the natural vibration modes of different regions to reinforce each other—this would result in peaks and troughs in the frequency response which were less numerous, but larger and less easily extinguished.

Experimental frequency responses measured directly in the cat have been presented. Comparison of the model results with these experimental data indicates that the damping can be fairly well represented by a mass-proportional damping coefficient on the order of $1\text{–}5\times10^{3}\ \mathrm{s}^{-1}$. This is consistent with other less direct experimental evidence cited in Sect. II C. It results in damping which is moderate at high frequencies and heavier at low frequencies.

## ACKNOWLEDGMENTS

This work was supported by the Medical Research Council of Canada, and by a joint Québec-Belgium travel grant. The experimental determination of the cat middle-ear response was carried out at the Fowler Memorial Laboratory of Columbia University. This part of the work was supported by NIH grants 5 RO1 NS 03654 and PO1 NS 22334, and by grant V4/235B from the National Scientific Research Foundation (Belgium).

## APPENDIX: PROGRAM IMPLEMENTATION DETAILS

At each time step, the displacement vector is calculated by a matrix inversion consisting of a forward reduction followed by a back substitution. As implemented in SAP IV, the back substitution involves a sequence of FORTRAN BACKSPACE's through a file containing the system stiffness matrix, which in general is too large to fit into high-speed memory. This turns out to be an extremely time-consuming operation under operating systems like VMS (or RSX on PDP-11's) which use file structures with variable-length records, since a BACKSPACE from record *n* to record *n-1* implemented as a REWIND followed by *n-1* READ's. This inefficiency has been avoided under the VMS operating system by creating an array of file-record pointers extracted from the operating system's internal file descriptors, and then using the system routine SYSSFIND to locate any required record. The same thing is accomplished under the RSX operating system using the system routines .MARK and .POINT. This modification is critical to the use of the direct-integration mode of SAP IV under these two operating systems.

Note that it has also been necessary to add a stop/restart capability to SAP IV to permit long simulations to be run overnight, stopped in the morning, and then restarted the next night. This requires that the set of all nodal displacements, velocities, and accelerations be saved at the end of the run and then be read in again as starting conditions.

Bathe, K. -J. (1982). *Finite Element Procedures in Engineering Analysis* (Prentice-Hall, Englewood Cliffs, NJ).

Bathe, K. -J., Wilson, E. L., and Peterson, F. E. (1974). "SAP IV. A structural analysis program for static and dynamic response of linear systems," Report No. EERC 73-11 (University of California, Berkeley).

Békésy, G. v. (1941). "On the measurement of the amplitude of vibration of the ossicles with a capacitive probe," Akust. Z. **6**, 1–16 (in German).

Békésy, G. v. (1960). *Experiments in Hearing*, translated and edited by E. G. Wever (McGraw-Hill, New York).

Decraemer, W. F., Maes, M. A., Vanhuyse, V. J., and Vanpeperstraete, P. (1980). "A non-linear viscoelastic constitutive equation for soft biological tissues, based upon a structural model," Biomech. **13**, 559–564.

Esser, M. H. M. (1947). "The mechanism of the middle ear: II. The drum," Bull. Math. Biophys. **9**, 75–91.

Frank, O. (1923). "Sound conduction in the ear," Sitzungsber. Math.-Phys. Kl. Bayer. Akad. Wiss. Munchen **1923**, 11–17 (in German).

Funnell, W. R. J., and Laszlo, C. A. (1978). "Modeling of the cat eardrum as a thin shell using the finite-element method," J. Acoust. Soc. Am. **63**, 1461–1467.

Funnell, W. R. J., and Laszlo, C. A. (1982). "A critical review of experimental observations on ear-drum structure and function," ORL J. Oto-Rhino-Laryngol. Relat. Spec. **44**, 181–205.

Funnell, W. R. J. (1983a). "On the undamped natural frequencies and mode shapes of a finite-element model of the cat eardrum," J. Acoust. Soc. Am. **73**, 1657–1661.

Funnell, W. R. J. (1983b). "Recent developments in modelling the eardrum and related structures using the finite-element method," in *Mechanics of Hearing* (Proc. IUTAM/ICA Symposium, Delft), edited by E. de Boer and M. A. Viergever (Nijhoff, The Hague, and Delft U. P., Delft), pp. 19–25.

Gran, S. (1968). "The analytical basis of middle-ear mechanics. A contribution to the application of the acoustical impedance of the ear," Dissertation, University of Oslo (in German).

Guelke, R., and Keen, J. A. (1949). "A study of the vibrations of the tympanic membrane under direct vision, with a new explanation of their physical characteristics," J. Physiol. **110**, 226–236.

Guinan, J. J., Jr., and Peake, W. T. (1967). "Middle-ear characteristics of anesthetized cats," J. Acoust. Soc. Am. **41**, 1237–1261.

Helmholtz, H. L. F. (1869). "The mechanism of the middle-ear ossicles and of the eardrum," Pflügers Arch. Physiol. (Bonn) **1**, 1–60 [in German; translated by A. H. Buck and N. Smith (Wood, New York, 1873) and by J. Hinton (New Sydenham Society, London, 1974), Vol. 62, pp. 97–155].

Khanna, S. M., and Tonndorf, J. (1972). "Tympanic membrane vibrations in cats studied by time-averaged holography," J. Acoust. Soc. Am. **51**, 1904–1920.

Khanna, S. M., and Stinson, M. R. (1985). "Specification of the acoustical input to the ear at high frequencies," J. Acoust. Soc. Am. **77**, 577–589.

Møller, A. R. (1961). "Network model of the middle ear," J. Acoust. Soc. Am. **33**, 168–176.

Nelson, F. C., and Greif, R. (1975). "Damping," in *Shock and Vibration Computer Programs. Reviews and summaries*, edited by W. Pilkey and B. Pilkey (Shock & Vibration Information Center, U.S. Dept. Defense, Washington, DC), pp. 603–623.

Onchi, Y. (1949). "A study of the mechanism of the middle ear," J. Acoust. Soc. Am. **21**, 404–410.

Onchi, Y. (1961). "Mechanism of the middle ear," J. Acoust. Soc. Am. **33**, 794–805.

Rabbitt, R. D., and Holmes, M. H. (1986a). "Formulation and analysis of a dynamic fiber composite continuum model of the tympanic membrane," in *Peripheral Auditory Mechanisms*, edited by J. B. Allen, J. L. Hall, A. Hubbard, S. T. Neely, and A. Tubis (Springer, Berlin), pp. 28–35.

Rabbitt, R. D., and Holmes, M. H. (1986b). "A fibrous dynamic continuum model of the tympanic membrane," J. Acoust. Soc. Am. **80**, 1716–1728.

Shaw, E. A. G. (1977). "Eardrum representation in middle-ear acoustical networks," J. Acoust. Soc. Am. 62, S12.
Singleton, R. D. (1979). "Mixed radix fast Fourier transforms," in *Programs for Digital Signal Processing*, edited by Digital Signal Processing Committee (IEEE, New York), pp. 1.4-1–1.4-18.
Stinson, M. R. (1985). "The spatial distribution of sound pressure within scaled replicas of the human ear canal," J. Acoust. Soc. Am. 78, 1596–1602.
Svane-Knudsen, V., and Michelsen, A. (1986). "The impulse response vibration of the human ear drum," in *Peripheral Auditory Mechanisms*, edited by J. B. Allen, J. L. Hall, A. Hubbard, S. T. Neely, and A. Tubis (Springer, Berlin), pp. 21–27.
Tonndorf, J., and Khanna, S. M. (1971). "The tympanic membrane as a part of the middle ear transformer," Acta Oto-Laryngol. 71, 177–180.
Wilkes, G. L., Brown, I. A., and Wildnauer, R. H. (1973). "The biomechanical properties of skin," CRC Crit. Rev. Bioeng. 1, 453–495.
Wilson, J. P., and Johnstone, J. R. (1975). "Basilar membrane and middle-ear vibration in guinea pig measured by capacitive probe," J. Acoust. Soc. Am. 57, 705–723.
Witnauer, L. P., and Palm, W. E. (1961). "Preliminary studies of dynamic mechanical properties of leather," Am. Leather Chem. Assn. J. 56, 58–67.
Zwislocki, J. (1957). "Some impedance measurements on normal and pathological ears," J. Acoust. Soc. Am. 29, 1312–1317.
Zwislocki, J. (1962). "Analysis of the middle-ear function. Part I: Input impedance," J. Acoust. Soc. Am. 34, 1514–1523.